AIAA JOURNAL
Vol. 44, No. 4, April 2006

Technical Notes

TECHNICAL NOTES are short manuscripts describing new developments or important results of a preliminary nature. These Notes should not exceed 2500 words (where a figure or table counts as 200 words). Following informal review by the Editors, they may be published within a few months of the date of receipt. Style requirements are the same as for regular contributions (see inside back cover).

Incompressible Flow Model of Synthetic Jet Actuators

Hui Tang* and Shan Zhong†
University of Manchester, Manchester, England M60 1QD, United Kingdom

I. Introduction

FOR flow control purposes, jet exit velocity, momentum flux, and vortex strength are among the important performance parameters that measure the impact of a synthetic jet on an external flow. To design suitable and effective synthetic jet actuators for a specific external flow, a simple but reliable model that is capable of predicting these parameters for a given actuator geometry and operating conditions is required.

Accurate prediction of the behavior of synthetic jets is challenging because of their complex unsteady nature. Some theoretical modeling work has been reported in the literature.[1,2] In these studies, the nondimensional parameters that determine the characteristic flow regimes of synthetic jets were identified. The effects of changing actuator geometry and operating conditions on the structure of synthetic jets were also investigated both experimentally and computationally.[3–8] The importance of dimensionless stroke length and Reynolds number in determining the characteristics of synthetic jets was confirmed. However, to the best knowledge of the authors, analytical models that can be used to predict the performance of synthetic jets quantitatively are still unavailable.

In the present work, a performance prediction model is developed for circular synthetic jet actuators in which the flow is assumed to be incompressible. Numerical simulations are conducted systematically to validate the model and to interpret the discrepancy between the predicted and simulated results. In the previous work by the authors, the numerical results from FLUENT were validated against hot-wire and particle image velocimetry (PIV) data. A good agreement between the prediction and the measurement was achieved in the form of the appearance of vortical structures, instantaneous centerline, and cross-stream velocity variations,[9] indicating the capability of FLUENT in reproducing the key features of synthetic jets. Because of the practical difficulties in obtaining accurate velocity profiles at the orifice exit plane using either a hot wire or PIV, as a first attempt to validate the prediction model, FLUENT is used when reliable experimental results are not yet available.

Presented as Paper 2005-104 at the AIAA 43rd Aerospace Sciences Meeting, Reno, NV, 10–13 January 2005; received 19 January 2005; revision received 29 July 2005; accepted for publication 4 November 2005.

*Research Student, School of Mechanical, Aerospace and Civil Engineering. Student Member AIAA.
†Senior Lecturer of Aerospace Engineering, School of Mechanical, Aerospace and Civil Engineering.

II. Theoretical Derivation

A. Dimensional Analysis

Consider a typical synthetic jet actuator shown in Fig. 1, which consists of a cylindrical cavity with a vibrating diaphragm at its bottom side and a circular orifice plate at the opposite side. The behavior of the synthetic jet depends on eight parameters: 1) diaphragm oscillation amplitude Δ, 2) diaphragm oscillation frequency f, 3) orifice diameter D_o, 4) orifice depth h, 5) cavity diameter D_c, 6) cavity depth H, 7) kinematic viscosity ν, and 8) fluid density ρ.

According to the Buckingham–Pi theorem, these parameters can be condensed into the following five independent nondimensional parameters that represent the actuator geometry and operating conditions:

$$\pi_1 = \Delta/D_o, \qquad \pi_2 = D_c/D_o, \qquad \pi_3 = H/D_o$$

$$\pi_4 = h/D_o, \qquad \pi_5 = f D_o^2/\nu$$

The performance parameters of synthetic jets, if expressed in their nondimensional form, are expected to be functions of these nondimensional parameters.

B. Parameters Describing the Performance of Circular Synthetic Jets

In the present study, it is assumed that the diaphragm is clamped round its edge and the peak-to-peak displacement at its center Δ is fixed at a known value. According to the theory of plates and shells,[10] the instantaneous shape of a diaphragm that undergoes a sinusoidal oscillation is described as

$$\delta(r,t) = (\Delta/2)\left[1 - \left(r^2/r_c^2\right) + \left(2r^2/r_c^2\right)\ln(r/r_c)\right]\cos(2\pi ft) \quad (1)$$

where δ is the diaphragm deformation relative to its neutral position, r is the radial distance from the center of the diaphragm, and r_c is the diameter of the diaphragm. The derivative of Eq. (1) with respect to time gives the oscillation velocity of the diaphragm:

$$u(r,t) = \pi\Delta f\left[1 - \left(r^2/r_c^2\right) + \left(2r^2/r_c^2\right)\ln(r/r_c)\right]\sin(2\pi ft) \quad (2)$$

For incompressible flows, based on mass conservation in the cavity, the instantaneous mass flow rate through the orifice is given by

$$\dot{Q}_o(t) = \rho\tilde{u}_o(t)A = \rho\int_0^{r_c} u(r,t)\cdot 2\pi r\,\mathrm{d}r$$

$$= \frac{\pi^2}{16}\rho\Delta f D_c^2\sin(2\pi ft) \quad (3)$$

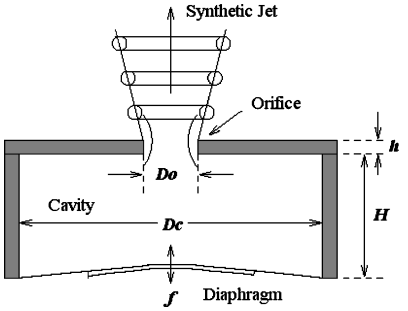

Fig. 1 Schematic of synthetic jet actuator.

where A is the cross-sectional area of the orifice. The instantaneous space-averaged velocity at the orifice exit becomes

$$\tilde{u}_o(t) = \dot{Q}_o(t)/\rho A = (\pi/4)\Delta f (D_c/D_o)^2 \sin(2\pi f t) \tag{4}$$

$\tilde{u}_o(t)$ forms the basis for estimating the jet performance parameters when the exit velocity profile is not readily available. Because $\tilde{u}_o(t)$ is independent of the orifice and cavity depth, the effect of changing H and h (or π_3 and π_4) cannot be included in the model.

From Eq. (4), the peak and the time-averaged blowing velocity over the entire cycle are found to be

$$\tilde{U}_{\text{peak}} = \frac{\pi}{4}\Delta f \left(\frac{D_c}{D_o}\right)^2 \tag{5}$$

$$\bar{U}_o = \frac{1}{T}\int_0^{T/2} \tilde{u}_o(t)\,\mathrm{d}t = \frac{1}{4}\Delta f \left(\frac{D_c}{D_o}\right)^2 \tag{6}$$

where T is the period of a diaphragm oscillation cycle. The total fluid mass flux and the time-averaged mass flow rate discharged through the orifice in a cycle are

$$Q_o = \int_0^{T/2} \dot{Q}_o(t)\,\mathrm{d}t = \frac{\pi}{16}\rho\Delta D_c^2 \tag{7}$$

$$\bar{\dot{Q}}_o = \frac{Q_o}{T} = \frac{\pi}{16}\rho\Delta f D_c^2 \tag{8}$$

When the space-averaged exit velocity $\tilde{u}_o(t)$ is used to replace the unknown exit velocity profile $u_o(r, t)$, the instantaneous momentum flux rate through the orifice can be approximated as

$$\dot{M}_o(t) = \rho\int_0^{r_o} u_o^2(r,t)\cdot 2\pi r\,\mathrm{d}r \approx \rho\tilde{u}_o^2(t)A$$

$$= \frac{\pi^3}{64}\rho\Delta^2 f^2 D_o^2\left(\frac{D_c}{D_o}\right)^4 \sin^2(2\pi f t) \tag{9}$$

Hence, the approximate total momentum flux or impulse I_o discharged during a cycle is

$$I_o = \int_0^{T/2} \dot{M}_o(t)\,\mathrm{d}t \approx \frac{\pi^3}{256}\rho\Delta^2 f D_o^2\left(\frac{D_c}{D_o}\right)^4 \tag{10}$$

and the approximate time-averaged momentum flux rate becomes

$$\bar{\dot{M}}_o = I_o/T \approx (\pi^3/256)\rho\Delta^2 f^2 D_o^2 (D_c/D_o)^4 \tag{11}$$

So far there is no accurate method of predicting the vortex circulation Γ. However, Γ can be estimated using the total circulation or the vorticity flux across the orifice exit Γ_o. According to Glezer,[11] this total circulation can be approximated as

$$\Gamma_o = \int \frac{u_o^2(0,t)}{2}\,\mathrm{d}t$$

Replacing $u_o(0, t)$ with the space-averaged velocity over the orifice $\tilde{u}_o(t)$ gives

$$\Gamma_o \approx \int_0^{T/2} \frac{\tilde{u}_o^2(t)}{2}\,\mathrm{d}t = \frac{\pi^2}{128}\Delta^2 f\left(\frac{D_c}{D_o}\right)^4 \tag{12}$$

C. Dimensionless Parameters Describing the Actuator Operating Conditions

The nondimensional stroke length and the Reynolds number have been identified as the two most important dimensionless parameters for describing the actuator operating conditions. The dimensionless stroke length is defined as $L = L_o/D_o$, where the stroke length L_o is the length of the fluid column expelled during the blowing cycle of a synthetic jet,[11] that is,

$$L_o = \bar{U}_o T \tag{13}$$

The Reynolds number is commonly defined as

$$Re = \bar{U}_o D_o/\nu \tag{14}$$

Substituting Eq. (6) into the definition of Reynolds number and L gives

$$L = \tfrac{1}{4}(\Delta/D_o)(D_c/D_o)^2 \tag{15}$$

$$Re = \tfrac{1}{4}(\Delta f D_o/\nu)(D_c/D_o)^2 \tag{16}$$

For a given synthetic jet actuator, L is proportional to the diaphragm displacement but independent of the oscillation frequency, whereas Reynolds number Re is proportional to the product of the diaphragm displacement and the oscillation frequency.

The dimensionless stroke length and Reynolds number are two independent dimensionless parameters on which the other dimensionless parameters depend. For example, the Strouhal number is the inverse of L, that is,

$$Sr = f D_o/\bar{U}_o = L^{-1} \tag{17}$$

whereas the Stokes number St is related to Reynolds number and L as

$$\mathrm{St} = (2\pi Re\cdot Sr)^{\frac{1}{2}} = (2\pi Re/L)^{\frac{1}{2}} \tag{18}$$

It can also be proved that the L and Reynolds number are related to the basic nondimensional parameters via

$$L = \tfrac{1}{4}\pi_1\pi_2^2, \qquad Re = \tfrac{1}{4}\pi_1\pi_2^2\pi_5 \tag{19}$$

D. Relationships Between the Performance Parameters and Operating Parameters

Combining Eqs. (5–12) with Eqs. (15) and (16) gives the relationships between the dimensionless jet performance parameters and Reynolds number and L. If D_o, f, and ρ are chosen as the basic parameters, $\bar{U}_o$, U_{peak}, $\bar{\dot{Q}}_o$, Q_o, $\bar{\dot{M}}_o$, I_o, and Γ_o are related to L and Reynolds number via

$$\bar{U}_o/fD_o = L \tag{20a}$$

$$\tilde{U}_{\text{peak}}/fD_o = \pi L \tag{20b}$$

$$\bar{\dot{Q}}_o\big/\rho f D_o^3 = (\pi/4)L \tag{20c}$$

$$Q_o\big/\rho D_o^3 = (\pi/4)L \tag{20d}$$

$$\bar{\dot{M}}_o\big/\rho f^2 D_o^4 \approx (\pi^3/16)L^2 \tag{20e}$$

$$I_o\big/\rho f D_o^4 \approx (\pi^3/16)L^2 \tag{20f}$$

$$\Gamma_o\big/fD_o^2 \approx (\pi^2/8)L^2 \tag{20g}$$

Alternatively, if D_o, ν and ρ are chosen as the basic parameters, the frequency f will not appear explicitly:

$$\bar{U}_o/(\nu/D_o) = Re \tag{21a}$$

$$\tilde{U}_{\text{peak}}/(\nu/D_o) = \pi Re \tag{21b}$$

$$\bar{\dot{Q}}_o/\rho\nu D_o = (\pi/4)Re \tag{21c}$$

$$Q_o\big/\rho D_o^3 = (\pi/4)L \tag{21d}$$

$$\bar{\dot{M}}_o\big/\rho\nu^2 \approx (\pi^3/16)Re^2 \tag{21e}$$

$$I_o\big/\rho\nu^2 D_o^2 \approx (\pi^3/16)Re\cdot L \tag{21f}$$

$$\Gamma_o/\nu \approx (\pi^2/8)Re\cdot L \tag{21g}$$

III. Computational Method

The actuator used in this study (Fig. 1) had a fixed geometry: $D_o = 45$ mm, $h = 5$ mm, $D_c = 45$ mm, and $H = 10$ mm. The diaphragm peak-to-peak displacement was allowed to vary from 0.3 to 1.1 mm with a 0.1-mm increment and the oscillation frequency from 50 to 400 Hz with a 50-Hz increment. A total number of 42 cases were simulated. Their operating conditions and the corresponding Reynolds numbers and dimensionless stroke lengths are listed in Table 1.

Unsteady two-dimensional axisymmetric incompressible numerical simulations were performed using a commercial solver FLUENT version 6.1. Figure 2 shows the computational geometry and mesh, as well as the boundary conditions. For simplification, a velocity-inlet boundary condition was applied at the neutral position of the diaphragm instead of a moving boundary condition. Previous study showed that this simplification had a negligible effect on the jet velocity and the formation of vortex rings. The time step used for the simulations was T/80. A sensitivity study undertaken previously confirmed that the choices of mesh size and time step used in the present study were adequate.[9] According to experimental observations, the near-field flow of all of the selected cases was laminar. Therefore, all of the simulations were conducted using the laminar model in the present study. Further details about the simulations can be found in Tang and Zhong.[9]

IV. Validation of the Model

Figure 3 shows the computed non-dimensional time-averaged mass flow rate $\bar{Q}_o$ at the orifice exit as a function of L or Reynolds number. The necessary result of the flow being incompressible, the nondimensional $\bar{Q}_o$ varies linearly with L or Reynolds number and follows exactly the same trend stated in Eqs. (20c) and (21c). As such, one would expect that the computed peak and time-averaged velocity at the orifice exit, $\bar{U}_{\text{peak}}$ and $\bar{U}_o$, also coincide with the prediction given by Eqs. (5) and (6).

According to Eqs. (20e) and (21e), the dimensionless time-averaged momentum flux rate $\bar{M}_o$ at the orifice exit should vary linearly with L^2 or Re^2. This trend appears to be well captured by FLUENT, except that the simulation result has a slightly larger slope (about 2.15) than the prediction ($\pi^3/16 \approx 1.94$) (Fig. 4a). In Fig. 4b, the computed nondimensional $\bar{M}_o$ for the same diaphragm displacement appears to lie along the same line. However, the slope of the line increases with Δ and gradually departs from the prediction.

Table 1 Case summary

	f, Hz								
Δ, mm	50	100	150	200	250	300	350	400	L
0.3	104	208	312	416	520	624	728	832	1.215
0.4	139	277							1.62
0.5	173	347	520	693	866	1040	1213	1386	2.025
0.6	208	416							2.43
0.7	243	485							2.835
0.8	277	555	832	1109	1386	1664	1941	2218	3.24
0.9	312	624							3.645
1.0	347	693							4.05
1.1	381	762	1144	1525	1906	2287	2669	3050	4.455

In the present study, the vortex circulation Γ is calculated by integrating the vorticity computed with FLUENT over a region containing a full vortex rollup, which is bounded by an isovorticity line of 20% of the maximum vorticity at the vortex center. Figure 5 shows the variations of the computed vortex circulation against L^2 and $Re \cdot L$, respectively. At lower values of L, the computed Γ follows the predicted total circulation Γ_o very well (Fig. 5a). However, Γ departs from Γ_o when $L > \sim 3.5$ and falls on to another straight line with a larger slope (dashed line, Fig. 5a). According to Eq. (20g) the slope of the predicted data is $\pi^2/8 \approx 1.23$. The slope of all of the simulated data has a value of 1.35 based on a linear best fit, and it is very close to the value of 1.30 found by Muller et al.[3] Figure 5b shows that Γ/ν varies with $Re \cdot L$ linearly and agrees with the prediction very well when $\Delta \leq 0.5$ mm. Although a good linear relationship between Γ/ν and $Re \cdot L$ still exists for larger Δ, the best-fit line departs from the prediction with the slope for $\Delta = 0.8$ mm below and that for $\Delta = 1.1$ mm above the predicted value. The linear relationship between Γ/ν and $Re \cdot L$ or L_o^2 have also been verified in experimental investigations.[11,12]

The discrepancy between the predicted and simulated momentum and vortex circulation is believed to be mainly caused by the

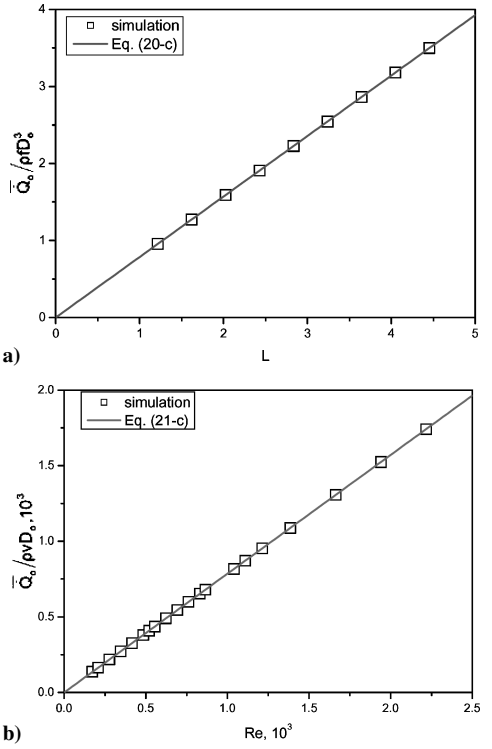

Fig. 3 Correlations between nondimensional time-averaged mass flow rate at the orifice exit during the blowing cycle and a) L and b) Reynolds number.

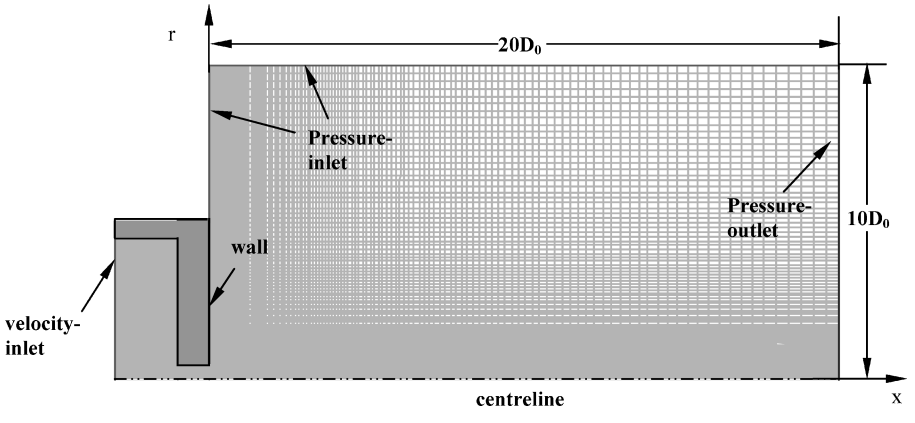

Fig. 2 Computational geometry, mesh, and boundary conditions.

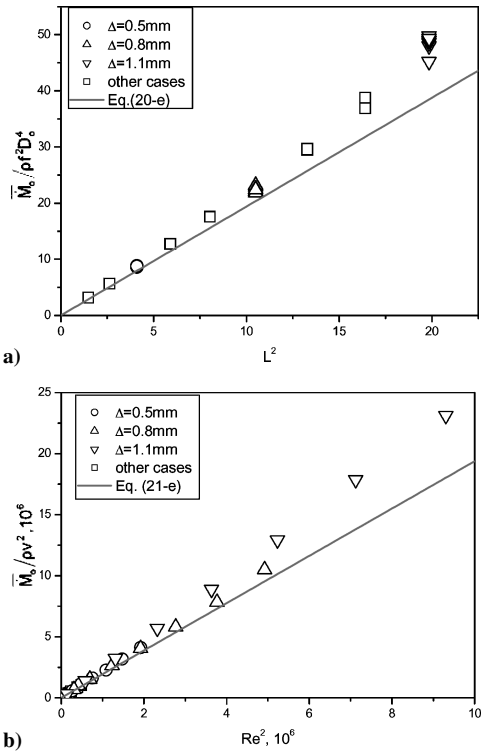

Fig. 4 Correlations between nondimensional time-averaged momentum flux rate at orifice exit during the blowing cycle and a) L^2 and b) Re^2.

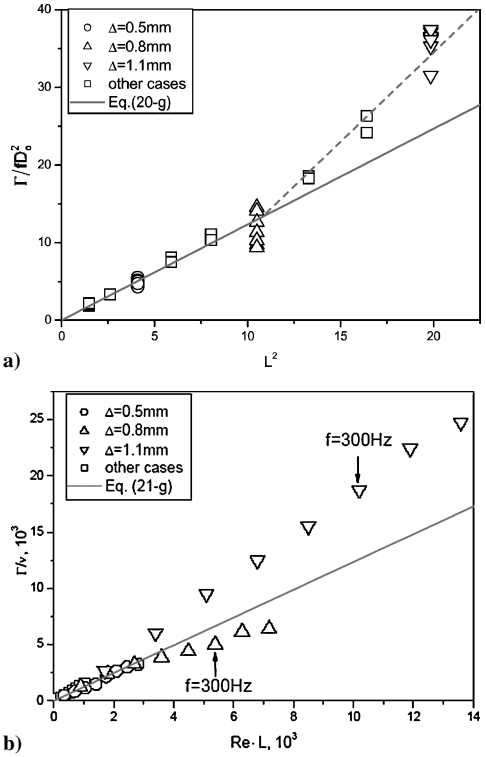

Fig. 5 Correlations between circulation and a) L^2 and b) $Re \cdot L$.

approximation associated with replacing the spatially varying exit velocity profile by the space-averaged velocity. It can be proved mathematically that the predicted momentum flux calculated in this way is always lower than the actual value as shown in Fig. 4. The normalized time-averaged exit velocity profiles during the blowing cycle for a range of diaphragm displacements at $f = 300$ Hz are shown in Fig. 6. It can be seen that at a lower Δ, the velocity in the core flow is lower than the space-averaged value due to the presence of a large velocity peak in the near-wall region. As

Table 2 P_M and $P_{\Gamma o}$ summary (f = 300 Hz)

	Δ, mm			
Variable	0.3	0.5	0.8	1.1
P_M	1.11	1.11	1.12	1.31
$P_{\Gamma o}$	0.77	0.84	0.94	1.56

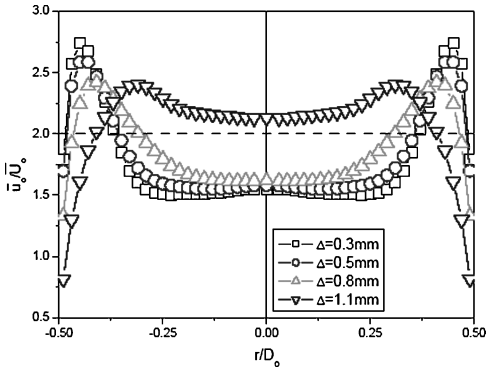

Fig. 6 Profiles of normalized time-averaged (during the blowing stroke) axial velocity at f = 300 Hz: - - - -, space-averaged value.

Δ increases, the velocity profile gradually transforms into a top-hat shape such that the velocity in the core flow becomes higher than the space-averaged value. Therefore, using the space-averaged velocity to replace the centerline velocity at the orifice exit [see Eq. (12)] is expected to underestimate the total circulation at 1.1 mm, whereas it overestimates that at the other three displacements. Nevertheless, the amount of discrepancy in the predicted and simulated vortex circulation may not be directly proportional to the difference between the space-averaged velocity and the centerline velocity at the orifice exit shown in Fig. 6. This could be because using the total circulation to estimate the vortex circulation is a simplification itself.

To account for the effects of this simplification, correction factors are introduced:

$$P_M = \frac{\bar{\dot{M}}_{o,\text{actual}}}{\bar{\dot{M}}_{o,\text{predicted}}} = \frac{\rho \int \overline{u_o^2(r,t)}\,\mathrm{d}A}{\rho \overline{\tilde{u}_o^2(t)} A} = \frac{(1/A)\int \overline{u_o^2(r,t)}\,\mathrm{d}A}{\overline{\tilde{u}_o^2(t)}} \tag{22}$$

$$P_{\Gamma o} = \frac{\Gamma_{o,\text{actual}}}{\Gamma_{o,\text{predicted}}} = \frac{\int_0^{T/2} \left[u_o^2(0,t)/2\right] \mathrm{d}t}{\int_0^{T/2} \left[\tilde{u}_o^2(t)/2\right] \mathrm{d}t} = \frac{\overline{u_o^2(0,t)}}{\overline{\tilde{u}_o^2(t)}} \tag{23}$$

where the upper bar denotes the time-averaged values during the blowing stroke. P_M and $P_{\Gamma o}$ for four different diaphragm displacements at $f = 300$ Hz are listed in Table 2. It is found that both P_M and $P_{\Gamma o}$ increase with Δ, which is consistent with the observation in Figs. 4 and 5. Making use of these correction factors, one can bring the predicted $\bar{\dot{M}}_o$ and $\bar{\Gamma}$ closer to the actual values and hence, extend the use of the model to higher stroke length. Nevertheless, further studies should be undertaken to establish the correlation between correction factors and the actual velocity profiles at the orifice exit.

V. Conclusions

A prediction model of circular synthetic jet actuators in which the flow is assumed to be incompressible is developed. This model provides analytical relations between the performance parameters and the operating/geometry parameters of synthetic jet actuators. The model was validated via a systematic numerical study for the range of $1.13 < L < 4.46$ and $104 < Re < 3050$. It is found that, for synthetic jets with relatively low values of dimensionless stroke length ($L < \sim 3.5$), the prediction is in a good agreement with the computed results. However, for jets with $L > \sim 3.5$, empirical correction factors have to be introduced to extend the use of the model. Although the analytical expressions presented in this Note are derived for circular synthetic jets, they can be easily extended to predict the behavior of synthetic jets from orifices of other shapes.

References

[1]Rathnasingham, R., and Breuer, K. S., "Characteristics of Resonant Actuators for Flow Control," AIAA Paper 96-0311, Jan. 1996.

[2]Lachowicz, J. T., Yao, C. S., and Wlezien, R. W., "Scaling of an Oscillatory Flow-Control Actuator," AIAA Paper 98-0330, Jan. 1998.

[3]Muller, M. O., Bernal, L. P., Miska, P. K., Washabaugh, P. D., Chou, T. A., Parviz, B. A., Zhang, C., and Najafi, K., "Flow Structure and Performance of Axisymmetric Synthetic Jets," AIAA Paper 2001-1008, Jan. 2001.

[4]Crook, A., "The Control of Turbulent Flows Using Synthetic Jets," Ph.D. Dissertation, School of Engineering, Univ. of Manchester, Manchester, England, U.K., Jan. 2002.

[5]Rizzetta, D. P., Visbal, M. R., and Stanek, M. J., "Numerical Investigation of Synthetic-Jet Flowfields," *AIAA Journal*, Vol. 37, No. 8, 1999, pp. 919–927.

[6]Lee, C. Y., and Goldstein, D. B., "Two-Dimensional Synthetic Jet Simulation," *AIAA Journal*, Vol. 40, No. 3, 2002, pp. 510–516.

[7]Utturkar, Y., Mittal, R., Rampunggoon, P., and Cattafesta, L., "Sensitivity of Synthetic Jets to the Design of the Jet Cavity," AIAA Paper 2002-0124, Jan. 2002.

[8]Shuster, J. M., and Smith, D. R., "A Study of the Formation and Scaling of a Synthetic Jet," AIAA Paper 2004-0090, Jan. 2004.

[9]Tang, H., and Zhong, S., "2D Numerical Study of Circular Synthetic Jets in Quiescent Flows," *Aeronautical Journal*, Vol. 109, No. 1092, 2005, pp. 89–97.

[10]Timoshenko, S., and Woinowsky-Krieger, S., *Theory of Plates and Shells*, 2nd ed., McGraw–Hill, London, 1959, pp. 67–69.

[11]Glezer, A., "The Formation of Vortex Rings," *Physics of Fluids*, Vol. 31, No. 12, 1988, pp. 3532–3542.

[12]Didden, N., "On the Formation of Vortex Rings: Rolling-Up and Production of Circulation," *Zeitschrift für Angewandte Mathematik und Physik*, Vol. 30, Jan. 1979, pp. 101–106.

K. Ghia
Associate Editor